JOURNAL OF APPLIED ELECTROCHEMISTRY 8 (1978) 179–193

Corrosion of nickel in sodium sulphate-sodium chloride melts. II. Potential-time and topochemical studies

C. A. C. SEQUEIRA, M. G. HOCKING

Metallurgy and Materials Science Department, Imperial College, London SW7, UK.

Received 31 May 1977

The corrosion behaviour of Ni in molten Na_2SO_4, NaCl, and in mixtures of these salts at 900° C, has been studied by electrochemical and topochemical methods. Microprobe analysis showed deep S penetration which causes embrittlement of the specimens by intergranular attack.

1. Experimental procedures

1.1. *Apparatus*

This has been described in Part I [1].

1.2. *Electrochemical Studies*

The passive-film breakdown experiments were performed as follows:(a) The polished working electrode was cathodically polarized for 5 min, immediately after immersion in the melt, at a potential 100–200 mV more negative than its free immersion potential; (b) After the interruption of the cathodization, the potential of the electrode was abruptly changed to a fixed passive potential and the electrode was kept at this potential for a certain time; (c) The spontaneous decay of the electrode potential was then recorded. The experimental runs were carried out for several passivation times and potentials. The circuit used for the current–time (and potential decay) measurements is similar to the circuit shown in Fig. 3 of Part I [1] except for the recorder, which was an *x–t* Smiths Servoscribe 2s recorder.

The cell used for measuring half-cell potentials versus Ag/Ag^+ (corrosimetric measurements) is similar to that schematically shown in Fig. 1 of Part I [1], with the difference that no counter-electrode is necessary.

The specimen, together with a silver–silver sulphate reference electrode, was suspended in either molten Na_2SO_4, NaCl or Na_2SO_4–NaCl mixtures contained in a crucible inside the furnace. Platinum leads from the specimen and reference electrode were connected to a Vibron Model 33B-2 high impedance electrometer or an Ekco vibrating reed electrometer type N616B and diagrams of the dependence of potential on time were recorded on an *x–t* Servoscribe plotter. The cell was filled with air or O_2/SO_2 mixtures and the e.m.f. measurements were started immediately upon immersion of the metal samples in the melt. The temperature was kept constant at about 900° C. An accuracy of ± 50 mV has been calculated for these long-run tested systems.

1.3. *Topochemical studies*

Nickel specimens exposed to Na_2SO_4–NaCl melts at 900° C under conditions of anodic potentiodynamic polarization and free corrosion, were examined by optical and steroscan electron microscopy techniques. In addition, and to further elucidate the effect of sodium chloride on the mode of anodic dissolution of nickel, a number of micrographs were prepared at various potentials. Each micrograph was obtained after the specimen had been polarized at a given potential at a constant charge of about 3·6 C cm^{-2}.

For both macro- and micrographic observations and photography a Reichert Universal Kamer Mikroskop 'Mef' was used; the SEM photographs were taken with the Steroscan Mark S600 (Cam-

bridge Scientific Instrument Co.).

Prior to these studies the exposed specimens were rinsed with water to take away the salt adhering to the specimen scale on removal from the crucible. For SEM observations the samples were stuck to the specimen stub by a conductive glue (Durofix). Micrography of the cross-sections (i.e., sections perpendicular to the sample surfaces) was done after setting the required specimen in araldite and dry polishing down to Oakey's Grade 4/0 paper and then on cartridge paper smeared with 0·25 μm diamond polishing paste.

Electron probe X-ray microanalyses (EPM) were then performed, to obtain a general film analysis and to attempt to study any concentration gradients.

In order to obtain more information about the $Ni/Na_2SO_4/NaCl$ reaction products, the soluble part of the residual melts and the powders collected at the top of the reaction cell at the end of an electrochemical experiment in chloride melts, were semiquantitatively analysed by X-ray fluorescence in a Philips 1220C spectrometer (heavy elements) and a JEOL SX-GO-11 spectrometer (light elements).

The solutions, according to solubility of the solidified melts, were dissolved in water to concentrations of either 120 $g\,l^{-1}$ or 30 $g\,l^{-1}$. The solid samples were prepared by pressing the powders into tablets with cellulose binder. This eliminates the variation in line intensity which may result from packing effects.

2. Results and discussion

2.1. *Electrochemical measurements*

2.1.1. Potential decay curves of passive nickel. The reproducibility of the curves obtained was in general poor; nevertheless, the curves fell into well-defined groups of conditions and some interesting conclusions can be derived from their shapes. Typical curves are presented in Figs. 1–3 to facilitate comparisons on the basis of differences in the passivation time and in the composition of the electrolyte.

It was noticed (Fig. 1) that if the nickel was polarized for very short time periods, i.e., for 1, 10 or 60 s in molten Na_2SO_4 in air then the potential decayed within seconds to a value approximately

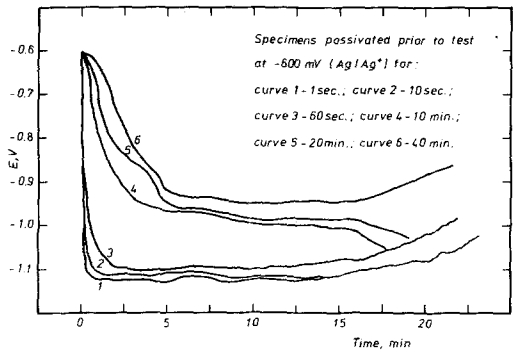

Fig. 1. Typical electrode potential decay curves for Ni specimens immersed in molten Na_2SO_4 at 900°C, in air.

corresponding to that of the immersion potential of Ni and remained at this value for about 15 min after which it slowly increased to more positive values. For nickel specimens passivated for 10–20 min the rate of the initial potential decay was much slower and potential plateaux were observed in the region of approximately − 1 V. Soon after the electrode potential reached a value of approximately − 1·05 mV, the potential–time curve showed a decrease in potential which gradually reached a value characteristic of a freely corroding electrode. It was also noticed that if the nickel was polarized for 30 min or more the potential increased after a more or less stable potential of approximately − 950 mV was reached.

The potential decay curves for nickel in molten Na_2SO_4–15% NaCl mixtures in air followed the same pattern as described above, with two important exceptions. Thin passive films (i.e., films which had grown for very short passivation times and therefore had not reached the steady state) were much more sensitive to Cl^- attack, the film reduction occurring quite instantaneously (Fig. 2). The potential 'arrest' regions were more pronounced than the potential plateaux observed in pure sulphate melts (Fig. 3). It therefore appears that once a thick oxide is formed on the surface of the nickel, the Cl^- addition is accompanied by an increase in the film stability. This is surprising since potentiodynamic polarization curves for nickel in Na_2SO_4–15% NaCl melts showed higher critical current densities than in pure Na_2SO_4. Hence, there appears to be no simple correlation between the ease of passivation and the stability of the passive film.

The inflection potential observed on the

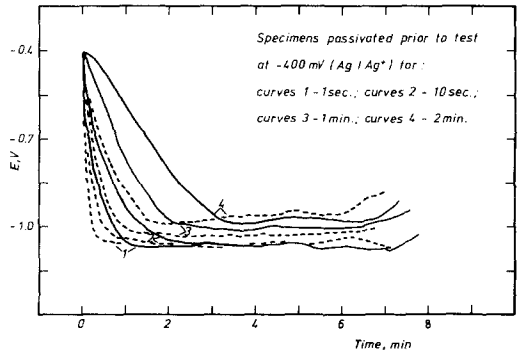

Fig. 2. Effect of the magnitude of the passivation time on potential decay characteristics of Ni in Na_2SO_4 (solid lines) and Na_2SO_4–15% NaCl (broken lines) melts at 900° C, in air.

potential decay curves is characteristic of a passive–active transition which is common in aqueous systems [2–5]; its value occurred below the primary passive potential observed on the polarization curve and will not necessarily correspond to the reversible potential of the nickel oxide/nickel electrode, since any potential in the decay curve is a mixed potential.

The abrupt film reduction observed after short-time passivation treatments indicates that a minimum time is required for the passive film to cover the whole metal surface. In all cases where a potential plateau was observed the relatively rapid potential decay after the interruption of the passivation process indicates that the most protective part of the passive film is that which is formed during the early stages of passivation. In the runs having longer passivation treatments, a gradual rise in potential occurred after a certain minimum value was reached, suggesting that a permanent passivity can be established by an adequate choice of the passivation time, which produces an equilibrium between the passive film and the electrolyte.

The fact that the oxide film renders the specimen passive and the non-coincidence of the primary passive potential observed on the polarization curve with the plateau potential observed on the potential decay, strongly suggest that the passivation of nickel takes place by a direct reaction of nickel with the electrolyte [6, 7], such as

$$Ni + SO_4^{2-} \rightarrow Ni\text{--}SO_3 + 1/2\ O_2 + 2e^-$$

followed by

$$Ni\text{–}SO_3 + SO_4^{2-} \rightarrow NiO + 2SO_3 + 2e^-.$$

On the other hand; the attainment of a single inflection suggests that the nickel forms only one oxide with quite likely the NiO lattice structure which may be either stoichiometric or non-stoichiometric.

2.1.2. Influence of NaCl on Ni in the transpassive area. Fig. 4 shows the *E/i* relationships of nickel obtained by the anodic potentiodynamic polarization method in Na_2SO_4 + NaCl melts at 900° C, in air, when the nickel specimens are in the overpassive region. The dissolution current is smaller in Cl^- melts than in SO_4^{2-} alone. In order to obtain further evidence of the protective effect of Cl^- ions in the transpassive region, Ni specimens were polarized at − 500 mV (Ag/Ag^+), held for 1 h at this potential, and then Cl^- was added and the current–time curves were recorded. For purposes of comparison, identical measurements were conducted in the absence of Cl^-. Fig. 5 shows that

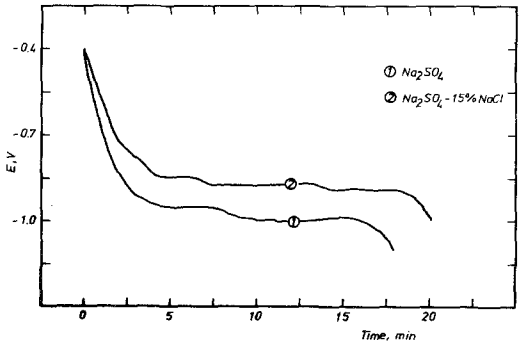

Fig. 3. Potential decay of Ni after 15 min polarization at − 400 mV in molten Na_2SO_4 and Na_2SO_4–15% NaCl mixtures at 900° C, in air.

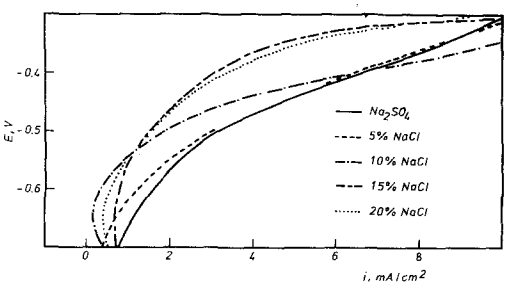

Fig. 4. Effect of NaCl on the potentiodynamic curves of the transpassive Ni in Na_2SO_4 at 900° C, in air.

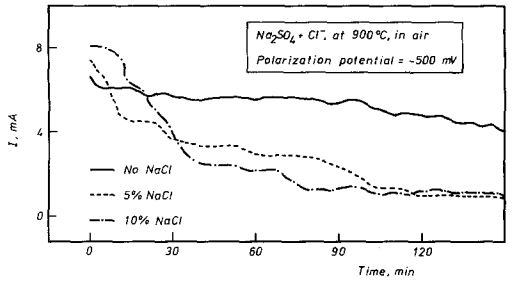

Fig. 5. Current–time curves of pure Ni at various Cl^- concentrations.

Cl^- inhibition, indicated by the decrease in current, predominates as the NaCl concentration increases.

In another series of experiments Ni specimens were passivated in pure Na_2SO_4 in air at 900° C at potentials in the overpassive area and held at these potentials for 1 h. NaCl was then added at a rate of 2 g per 5 min, and the current–time curves were measured. The considerable fall in current (see Fig. 6) shows that the inhibiting effect can predominate even when the overpassive potential is relatively high.

Present results were as expected from the potentiodynamic polarization studies and substantiate the previous conclusion that two competing processes take place on nickel in the passive–overpassive area, i.e. breakdown of the passive film and its formation by Cl^-.

2.1.3. Free corrosion potential measurements of Ni. When a nickel electrode is placed in molten sodium sulphate, freezing of the salt around the specimen occurs for about 10 s, and no electrode potential can be read. Once the salt is melted around the specimen a potential is read which normally is more positive than the highly negative potential which is observed after a few minutes of immersion. This active potential may be attributed to a mixed electrode process described by Reactions 2 and 3 of Part I [1], which are accompanied by the direct adsorption of the SO_3 species at the electrode interface (see Part I [1] on the dissolution and passivation of Ni in Na_2SO_4)

$$SO_4^{2-} + Ni \rightarrow Ni\text{--}SO_3 + 1/2\ O_2 + 2e^-.$$

The subsequent rise of potential would result from the dissolution of nickel and the formation of nickel oxide by processes such as

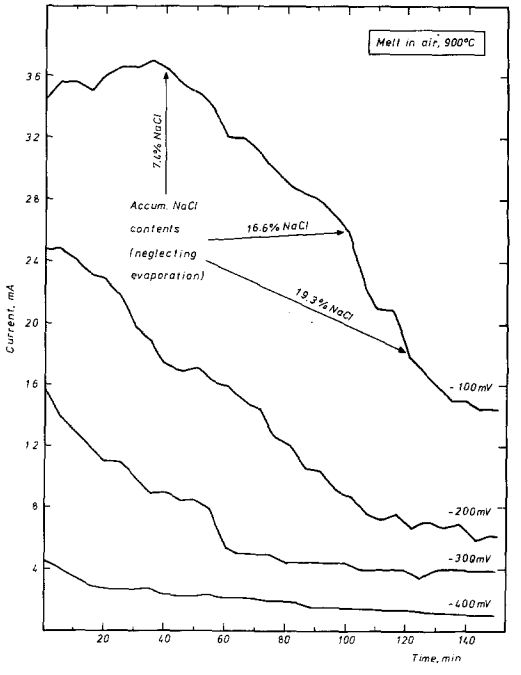

Fig. 6. Currents of nickel electrodes as a function of time on addition of NaCl to Na_2SO_4.

$$Ni\text{--}SO_3 + SO_4^{2-} \rightarrow NiO + 2SO_3 + 2e^- \quad (1)$$

and

$$Ni\text{--}SO_3 \rightarrow Ni^{2+} + SO_3 + 2e^-. \quad (2)$$

Typical potential–time curves are shown in Figs. 7 and 8. It is clear that the tendency of the nickel electrode is to become a Ni, NiO/O^{2-} electrode on approaching the redox potential of the melt, which is approximately − 180 mV in molten Na_2SO_4 in air [8].

The nickel potential attains a relatively stationary state 30–35 h after immersion. This means that no further changes in composition occur at the oxide–electrolyte interface.

The effect of the NaCl on the nickel electrode potentials is also shown in Figs. 7 and 8. Addition of NaCl decreases the oxide ion content of the melt, and consequently the first measured potentials are more positive than in sulphate alone. However the duration of the first potential shift towards more active potentials is longer and the gradual ennoblement up to a relatively steady-state potential occurs very slowly suggesting that the establishment of a Ni, NiO/O^{2-} electrode in sulphate–chloride melts is more difficult to achieve. This effect of NaCl on the equilibrium rate, through a film inhibiting action, suggests a

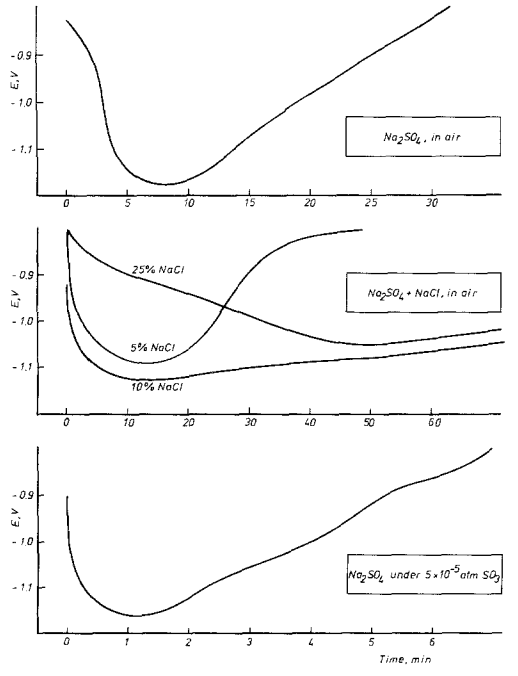

Fig. 7. Potential of nickel electrodes immersed in Na_2SO_4–NaCl melts at 900° C as a function of time for the first minutes of immersion.

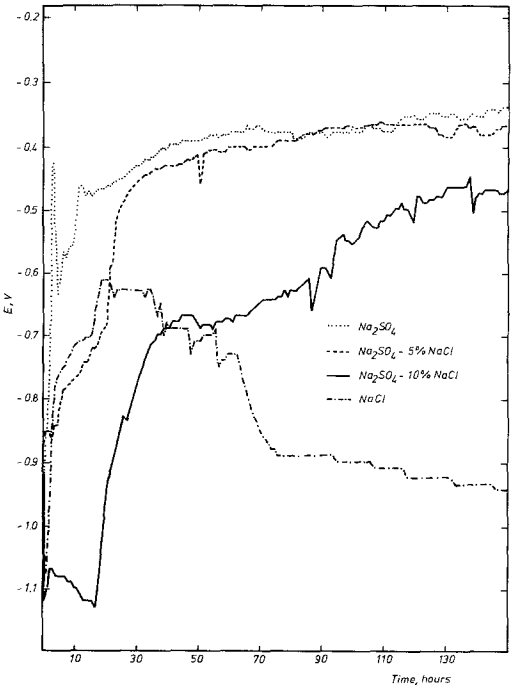

Fig. 8. Time–potential curves for nickel electrodes in Na_2SO_4–NaCl melts at 900° in air.

Ni–Cl^- species which is sufficiently stable to lower the Ni^{2+} concentration. Clearly, once the filming reaction succeeds in controlling the electrode potential, the nickel electrode works close to a redox one, its potential depending on the activity of the oxygen ions in the melt and probably of the ions in the oxide phase.

Thus, nickel upon interaction with sulphate–chloride melts is converted into an oxide electrode, the initiation of the screening reaction depending on the chloride ion content in the system. In pure sodium chloride (Fig. 8) the nickel electrode potential shifts initially towards more noble values but after some time of immersion changes to more negative potentials which are associated with corrosion taking place (as supported by visual observations that the nickel oxide did not accumulate at the metal surface and of distinct traces of disruption at the grain boundaries).

The effect of the SO_3 atmosphere on the nickel electrode potentials is shown in Fig. 9. Addition of sulphur trioxide decreases the rate of the thermal dissociation of sulphate ions

$$SO_4^{2-} = SO_3 + O^{2-}. \qquad (3)$$

The activity of oxygen ions in the melt decreases and the free corrosion potentials of the nickel specimens studied shift in the noble direction. In sodium sulphate melts under 10^{-1}–5×10^{-3} atm SO_3, the potential measured immediately after immersion may represent an overall process described by the reaction

$$Ni + SO_3 = Ni^{2+} + SO_2 + O^{2-}. \qquad (4)$$

Based on the 'Erdey–Gruz–Volmer' theory and on the 'acid–base' concept of Lux [9] and Flood *et al.* [10], it is easy to show that for Reaction 4 the following relationship between the corrosion potential and the function $pO^{2-} = -\log \{O^{2-}\}$ can be deduced

$$E_c = \frac{2{\cdot}3RT}{[\alpha + (1-\alpha')]F} \log \frac{A'k'K_e}{Ak\{Ni\}} + \frac{2{\cdot}3RT}{[\alpha + (1-\alpha')]F} O^{2-}$$

where A is the sink area and A' is the electron source area (at the interface nickel–sodium sulphate), $\{Ni\}$ is the activity of the nickel atoms immediately at the electrode surface (unity), α

and α' are the transfer coefficients for the reactions

$$Ni \rightarrow Ni^{2+} + 2e^- \quad (5)$$

and

$$SO_3 + 2e^- \rightarrow SO_2 + O^{2-} \quad (6)$$

respectively, k and k' are the chemical rate constants for Reactions 5 and 6 respectively, and K_e is the equilibrium constant for Equation 3 (K_e at 1173 K is equal to $10^{-19{\cdot}57}$). In Fig. 10 the nickel electrode potentials which were read immediately after the salt melted around the specimens, are plotted as a function of the SO_3 partial pressure over the melt or the pO^{2-} of the melt which is related to the SO_3 partial pressure by the expression

$$O^{2-} = 19{\cdot}57 + \log P_{SO_3}$$

(at unit sulphate-ion activity).

It is seen that a linear relationship between the initial free corrosion potential of the nickel electrode and the pO^{2-} of the melt is attained, from which some essential parameters of the mixed process (Reaction 4) may be derived. Since, at 900° C, $2{\cdot}3RT/F = 0{\cdot}2326$ V, and $\alpha + \alpha'$ may be assumed to be equal to unity, from $2{\cdot}3RT/[\alpha + (1-\alpha')]F = 0{\cdot}405$ V it can be estimated that $\alpha = 0{\cdot}275$ and $\alpha' = 0{\cdot}725$. Moreover, from

$$\frac{2{\cdot}3RT}{[\alpha + (1-\alpha')]F} \log \frac{A'k'K_e}{Ak\{Ni\}} = -8{\cdot}148 \text{ V}$$

and assuming that $A = A'$ and $\{Ni\} = 1$, it follows that $k'/k = 10{\cdot}67$. This means that at the instant of immersion the de-electronation process (Reaction 5) is controlling the corrosion rate.

The subsequent rapid change of the nickel electrode potentials to more positive values shows that Reaction 4 is no longer operative, i.e., under the high SO_3 atmospheres used it is unstable and another process should take place. This is in agreement with the potential/pO^{2-} diagram for nickel–sodium sulphate at 900° C [8], from which it can be deduced that the process which would then be set up is

$$NiS + 3O^{2-} = Ni^{2+} + SO_3 + 8e^-. \quad (7)$$

Table 1 shows the nickel electrode potential values measured after 5 min of immersion in pure sodium sulphate as a function of pO^{2-}. This shows that the electrodes obey the Nernst equation

$$E = E^\circ + 0{\cdot}0291 \log \{Ni^{2+}\} + 0{\cdot}1163pO^{2-}$$

for Equation 7. Once more, however, this reaction appears to be potential-determining owing to the conjugate cathodic reactions, Reaction 6 and

$$1/2\ O_2 + 2e^- = O^{2-} \quad (8)$$

which would establish a mixed process at the electrode, its potential continuing increasing until the redox potential of the melt is approached (see Fig. 9). A stationary state is obtained in 10–100 min depending on the SO_3 partial pressure over the melt.

The results of our potentiodynamic studies in Part I [1] show that SO_3 increases the corrosion rate of pure nickel immersed in molten sodium sulphate. Present corrosometric findings show clearly that SO_3 shifts the corrosion potential in the noble direction. Thus, depolarization of the cathodic reaction (conjugate of the corrosion reaction) should occur as is schematically shown in Fig. 11.

Table 1. Variation of the nickel electrode potentials, measured 5 min after immersion in molten sodium sulphate, with the pO^{2-} of the electrolyte

pO^{2-}	*Ni potential versus* Ag/Ag^+ (mV)	*Observed shift* (mV)	*Calculated shift:* $(2{\cdot}3RT/2F)pO^{2-}$ (mV)
18·61	−520	0	0
18·62	−515	−5	−1·2
18·52	−520	0	10·5
18·42	−540	20	22·1
18·20	−570	50	47·7
17·82	−630	110	91·9
17·30	−680	160	152·4

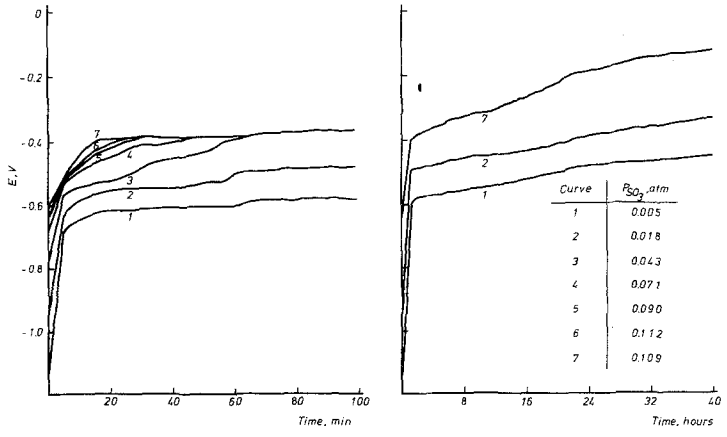

Fig. 9. Time–potential curves for nickel electrodes in molten sodium sulphate at 900° C under several SO_3 atmospheres.

3. Observations and analyses

3.1. *Micrography studies and electron probe microanalyses*

An idea of the topochemical results on nickel can be gained by scanning Figs. 12–15 and 17–35. However, verbal description must be added to give a more complete picture of specimen surface condition and this is given, with other information, below.

3.1.1. Potentiodynamically polarized samples. The following observations were made on specimens removed from the melt after forward and backward sweeps.

(i) Ni, Na_2SO_4, air: Dark yellowish green, surface attack fairly uniform (Fig. 12). Light grain boundary penetration, voids and few Ni islands. The SEM micrograph shown in Fig. 13 shows oxide crystals growing on the Ni surface. S was not found either in the voids, or anywhere in the metal–oxide system. O was also undetectable.

(ii) Ni, Na_2SO_4–15% NaCl, air: Uniform field and presence of scratches indicating more dissolution of the surface corrosion products (Fig. 14). Heavy internal grain boundary attack, plus a few pits. Oxides can be observed growing along scratch lines (Fig. 15). Fig. 16 shows a typical Ni section. No S, Cl or Na were detected either in the voids or in the external NiO porous fragile layer (which is almost always green). Ni_3S_2 was identified (see Fig. 16). NiO and Ni_3S_2 are, therefore, the main corrosion products. Absorbed electron images (AEI) of a corrosion pit are shown in Figs. 17–19; a sulphur X-ray image of the region shown in Fig. 17 is given in Fig. 18. The Ni, S and O contents of this region were determined. The oxygen content was below the detection limit of the electron probe. S and Ni countings were made using CdS and pure Ni as standards. The results showed that the material was not homogeneous, being higher in sulphur near the outer surface (see Fig. 16), so the measurements were split into two (Outer and Inner), before calculating the corrected values. The results are given in Table 2.

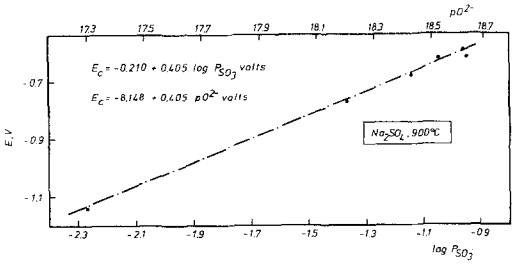

Fig. 10. Effect of P_{SO_3} on the nickel electrode potentials at the very first stage of any reaction with the molten salt.

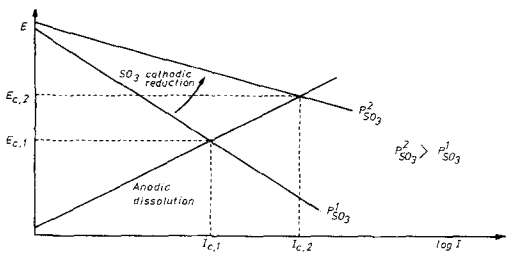

Fig. 11. Effect of sulphur trioxide pressure on the E, i characteristics of nickel in molten sodium sulphate.

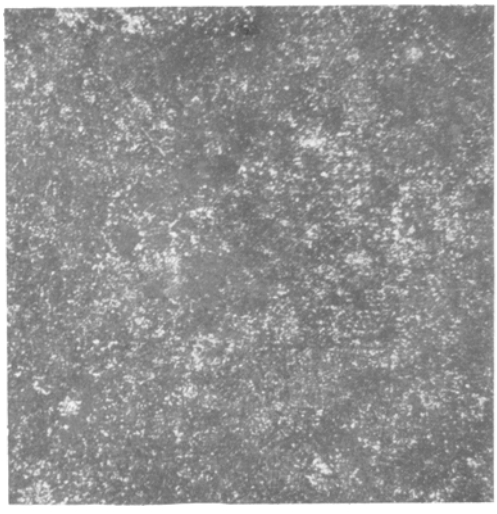

Fig. 12. Ni after potentiodynamic sweep in molten Na_2SO_4 at 900° C, in air. Surface (× 35).

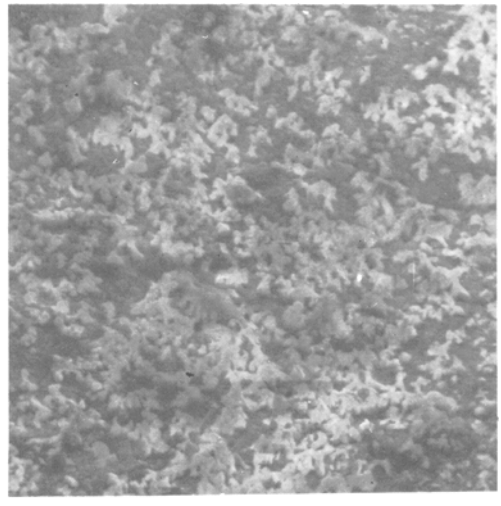

Fig. 13. Conditions as in Fig. 12. Surface (SEM) (× 1070).

The outer zone consists, therefore, of a network of Ni_3S_2 and the inner zone consists of a mixture of Ni and Ni_3S_2; it is probably this Ni–Ni_3S_2 liquid eutectic structure at 900° C which undermines the exposed metal making the corrosive process more extensive and, consequently, originating deep perforations.

(iii) Ni, Na_2SO_4–80% NaCl, air: Heavy grain boundary attack and indications of strong dissolution.

(iv) Ni, NaCl, air: Heavy attack with cracks across scale (Fig. 20), which is mainly dark green. A cross-section reveals severe intergranular attack. Pure Ni islands and bits of NiO were found everywhere at the surface. SEM micrographs show enhancement of corrosion along the grain boundaries (Fig. 21). The Na content at the surface was 2–3%; neither Na nor Cl were found in the voids.

(v) Ni, Na_2SO_4, 5×10^{-5} atm SO_3: Dark Greenish-gray, slight corrosion attack, grain boundary grooving.

Table 2.

	Sulphur		*Nickel*	
Location	(wt%)	(at.%)	(wt%)	(at.%)
Inner region	19·4	30·5	80·6	69·5
Outer region	27·0	40·4	73·0	59·6

(vi) Ni, Na_2SO_4–15% NaCl, 5×10^{-5} atm SO_3: Severe corrosion showing unreacted Ni islands (Fig. 22). Evidence of internal attack.

(vii) Ni, Na_2SO_4–50% NaCl, 5×10^{-5} atm SO_3: Similar to (vi) with more etch.

(viii) Ni, Na_2SO_4, 0·11 atm SO_3: Evidence of corrosion with light dissolution (Fig. 23); grain boundary attack. SEM shows formation of blistered products; note a grain boundary outlined by corrosion in Fig. 24. Microprobe analysis showed the presence of pure Ni fragments at the base metal, and sulphur particles in the outer part of the scale.

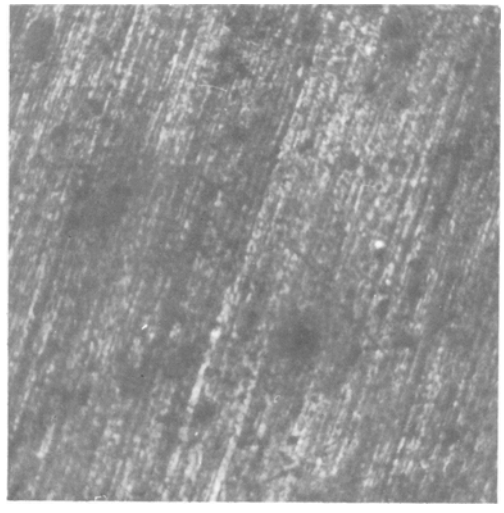

Fig. 14. Ni after potentiodynamic sweep in molten Na_2SO_4–15% NaCl at 900° C, in air. Surface (× 35).

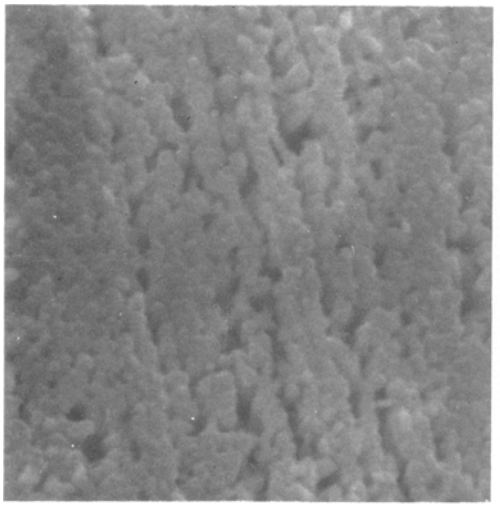

Fig. 15. Conditions as in Fig. 14. Surface (SEM) (× 5350).

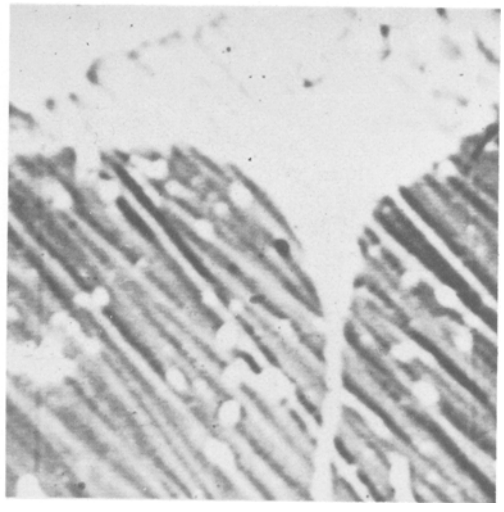

Fig. 17. Ni, 900° C, Na_2SO_4–15% NaCl in air after potentiodynamic sweep AEI (× 1200): close view of one end of a corrosion pit.

3.1.2. Freely corroded samples. The following observations were made.

(i) Ni, Na_2SO_4, air, 140 h: Dark green, fairly uniform corrosion layer consisting of NiO, mainly. Particles of unreacted nickel were found beneath the oxide layer. No evidence of sulphide formation was observed.

(ii) Ni, Na_2SO_4–10% NaCl, air, 140 h: Similar to above. Voids, nickel sulphide particles and unreacted nickel islands were found on the metal beneath a continuous thin layer of NiO.

(iii) Ni, NaCl, air, 140 h: Uniform surface, intergranular corrosion. SEM showed that the corrosion scale consists of Ni fragments beneath a thin NiO layer. Neither Na nor Cl were detected.

(iv) Ni, Na_2SO_4, 5×10^{-3} atm SO_3, 100 h: Uneven surface (Fig. 25), severe corrosion with internal penetration (Fig. 26). The surface morphology of the specimen is irregular and broken; thin plates (or flakes) are found scattered everywhere (Fig. 27). Electron probe showed a corrosion layer consisting mainly of pure nickel islands intermingled with sulphide particles and probably oxide; at the nickel matrix sulphide particles were detected.

(v) Ni, Na_2SO_4, 0·11 atm SO_3, 40 h: Similar to above with more penetration. Probe analysis indicated sulphur diffusion into the metal.

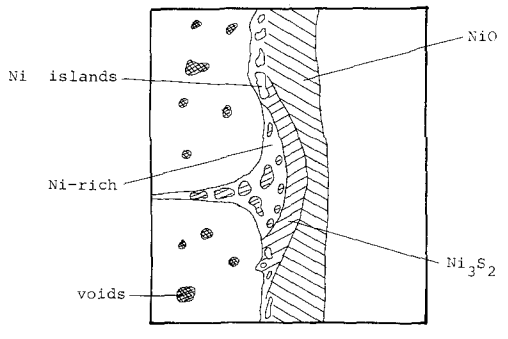

Fig. 16. Diagram of typical Ni section.

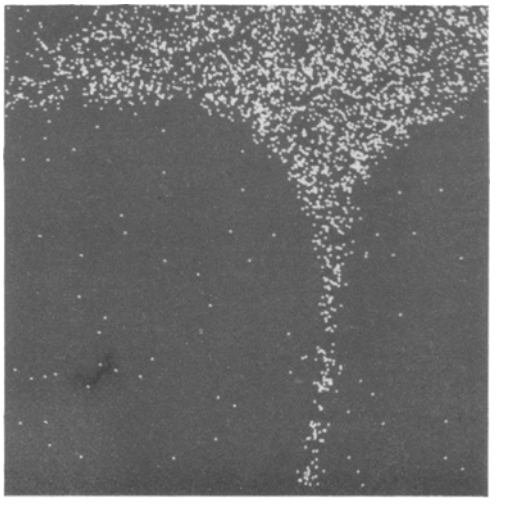

Fig. 18. Conditions as in Fig. 17, X-ray image (× 1200): distribution of S.

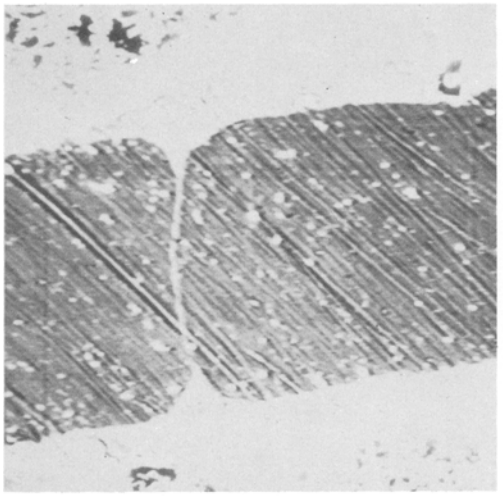

Fig. 19. Conditions as in Fig. 17, AEI (× 300): complete view of corrosion pit.

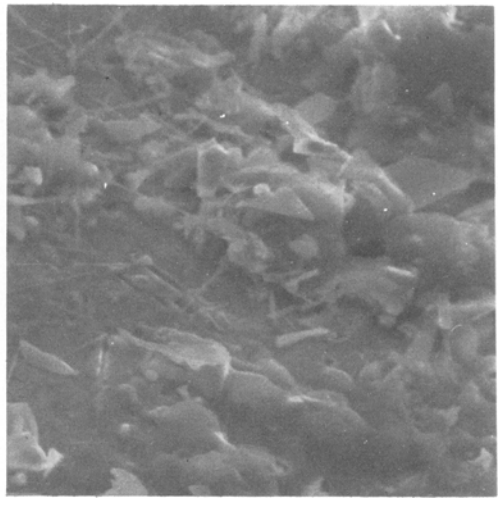

Fig. 21. Conditions as in Fig. 20. Surface (SEM) (× 1070).

3.1.3 Potentiostatically polarized samples. The following observations were made.

(i) Ni, Na_2SO_4, air, − 1·0 V (Fig. 28, A): Surface dissolution especially along the grain boundaries. Note the heavy etching shown in Fig. 29. The corrosion layer consists of unreacted Ni islands (see Fig. 30) and NiO. S was not detected.

(ii) Ni, Na_2SO_4, air, − 0·7 V (Fig. 28, B): Light corrosion, thin film covering scratches (Fig. 31). The general retention of smoothness indicates that the oxide film is formed on the whole surface allowing only random dissolution of the nickel as in the case of electrochemical polishing.

(iii) Ni, Na_2SO_4, air, − 0·5 V (Fig. 28, C): Moderate corrosion. Evidence of scratches indicating little corrosion and some film dissolution (Fig. 32).

(iv) Ni, Na_2SO_4, air, − 0·1 V (Figs. 28, D): Similar to above with more dissolution. The scratches found at − 0·5 V were no longer visible, as indicated in Fig. 33. The scale contains metallic particles of Ni in a NiO matrix. Neither Na nor S were detected.

(v) Ni, Na_2SO_4–15% NaCl, air, − 0·85 V (Fig. 28, E): Considerable corrosion with intense attack at grain boundaries (Fig. 34). Tiny spots of

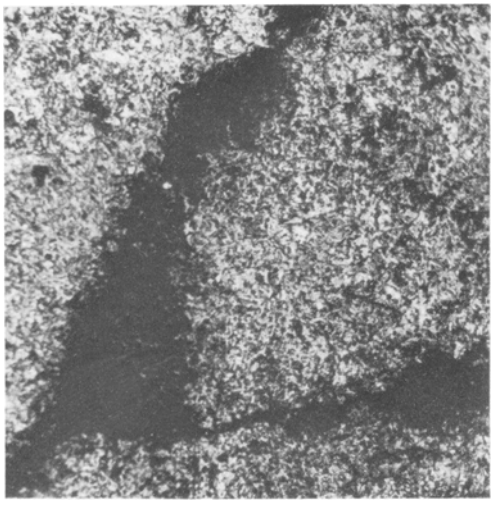

Fig. 20. Ni after potentiodynamic sweep in molten NaCl at 900°C, in air. Surface (× 35).

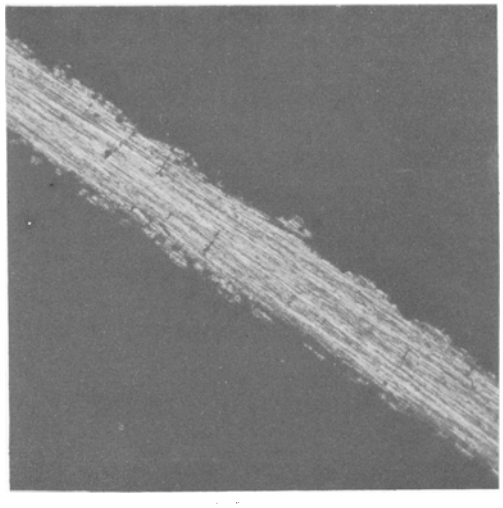

Fig. 22. Ni, 900° C, Na_2SO_4–15% NaCl, 0·00005 atm SO_3, after potentiodynamic sweep, section (× 48): severe corrosion showing unreacted Ni islands.

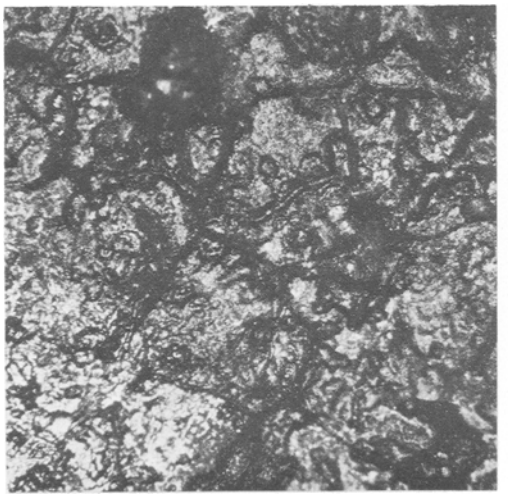

Fig. 23. Ni after potentiodynamic sweep in molten Na_2SO_4 at 900° C, under 0·11 atm SO_3. Surface (X 35).

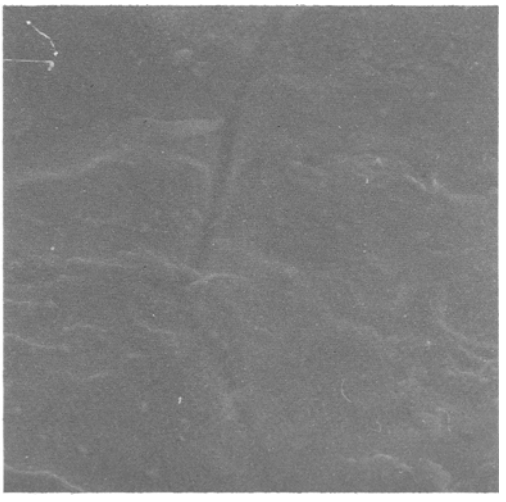

Fig. 24. Conditions as in Fig. 23. Surface (SEM) (X 535).

high Na content were found in addition to the corrosion products observed in (i).

(vi) Ni, Na_2SO_4–15% NaCl, air, − 0·6 V: Similar to (ii) showing practically complete retention of smoothness. Neither Na and Cl, nor S were detected, only Ni and NiO.

(vii) Ni, Na_2SO_4–15% NaCl, air, − 0·4 V: Similar to (iii).

(viii) Ni, Na_2SO_4–15% NaCl, air, − 0·2 V (Fig. 28, F): Similar to (iv) with more etch grain boundary attack (Fig. 35).

3.2. *X-ray fluorescence results*

Spectroscopic investigation of the enormous quantities of powders, which normally condensed

Table 3. Spectroscopic analysis of soluble residual melts and corrosion powder pellets (wt%)

Element	*Sample1*	*Sample 2*	*Sample 3*	*Sample 4*
Na	ND*	> 5	ND	> 5
S	> 5	> 5	> 5	> 5
Cl	> 5	> 5	ND	> 5
K	< 0·05	0·05–0·5	< 0·05	0·05–0·5
Ca	0·05–0·5	< 0·05	< 0·05	< 0·05
Ti	< 0·05	< 0·05	< 0·05	< 0·05
Cr	< 0·05	< 0·05	< 0·05	< 0·05
Fe	0·05–0·5	< 0·05	< 0·05	0·05–0·5
Co	ND	ND	ND	ND
Ni	ND	0·05–0·5	0·05–0·5	0·05–0·5
Cu	ND	< 0·05	ND	ND
Zr	< 0·05	< 0·05	< 0·05	< 0·05
Rb	ND	< 0·05	ND	ND
Mo	ND	ND	ND	ND
Ag	ND	< 0·05	ND	ND
Cd	ND	ND	ND	ND
Sr	ND	ND	ND	ND
I	ND	< 0·05	ND	ND
Cs	< 0·05	< 0·05	ND	ND
Pb	ND	< 0·05	ND	ND

* ND ≡ not detected. The window used in solution techniques effectively cancels all sodium radiation.

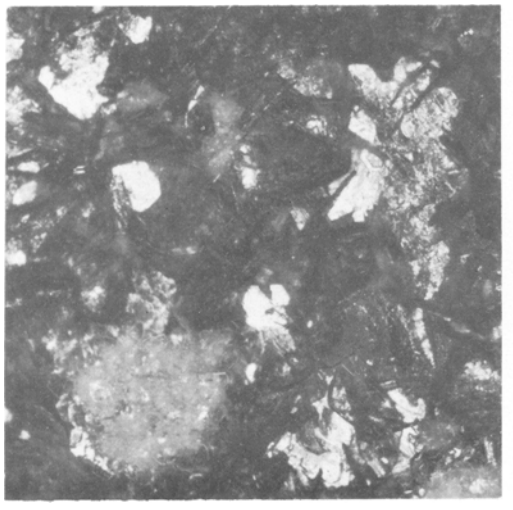

Fig. 25. Surface appearance of the scale formed on Ni immersed in molten Na_2SO_4 for 100 h at 900° C under 1 atm O_2 and 0·005 atm SO_3. (× 35).

on the inner pyrex top and walls of the high-temperature cell used during this work on electrochemical corrosion studies in Cl-containing melts, showed that their major constituents are Na, Cl, S, Ni, and K. Evaporation of S-containing compounds (from the sulphate dissociation and/or the inlet gas mixture), NaCl, $NiCl_2$, Na_2O and K_2O which is favoured under the experimental conditions might be responsible for such condensation at the cooler parts of the apparatus.

Typical results of the spectroscopic analysis

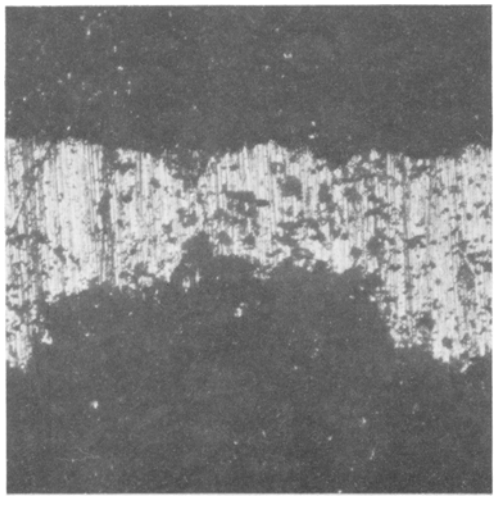

Fig. 26. Ni, 900° C, Na_2SO_4, 1 atm O_2 and 0·005 atm SO_3, 100 h, section (× 152): severe corrosion with internal penetration.

Fig. 27. Conditions as in Fig. 25. Surface (SEM) (× 1070).

are listed in Table 3. All the results in this table are calculated back to the original solid materials. Sample 1 is of the residual melt used for a potentiodynamic experiment of Ni in Na_2SO_4–15% NaCl, in air; Sample 2 consists of powder collected at the furnace top at the end of a 120 h corrosimetric test of Ni in Na_2SO_4–10% NaCl, in air; Sample 3 is of the Na_2SO_4 melt where Ni was corroded for 120 h, in 5×10^{-5} atm SO_3; Sample 4 contains powder condensed at the cooler top of the cell after a potentiodynamic test of Ni in Na_2SO_4–50% NaCl, under 5×10^{-5} atm SO_3.

3.3. *Discussion of topochemical studies*

(a) Pure Na_2SO_4 in air does not seem to be very corrosive to Ni.

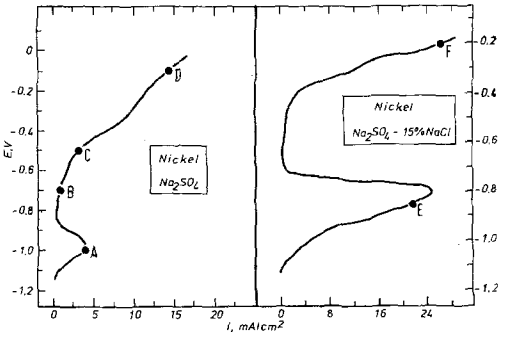

Fig. 28. E–i relationships for Ni in Na_2SO_4 and Na_2SO_4–15% NaCl mixtures at 900° C, in air, showing conditions at which some specimens were treated for microscopical and electron probe examinations.

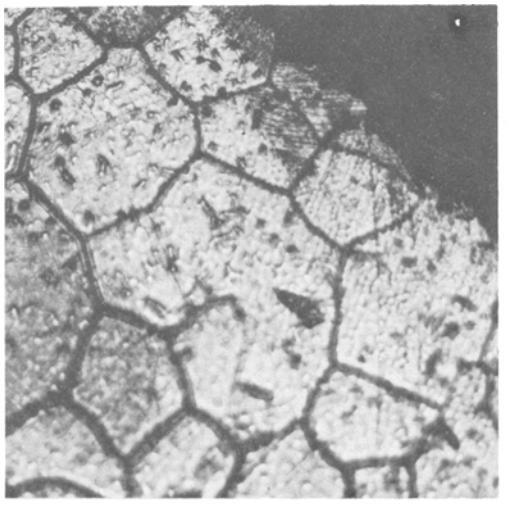

Fig. 29. Dissolution of Ni in the active potential range (— 1·0 V) in Na_2SO_4 at 900° C, in air (A, Fig. 28). Surface (× 35).

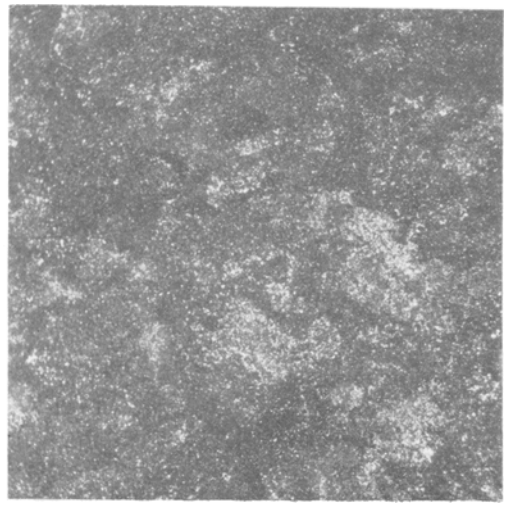

Fig. 31. Dissolution of Ni between passivation and transpassivation potential (— 0·7 V) in Na_2SO_4 at 900° C, in air (B, Fig. 28). Surface (× 35).

(b) Addition of NaCl to the molten Na_2SO_4 results in enhancement of attack over most of the nickel surface and there are indications of the start of selective attack (i.e. grain boundaries and pits). Based on the equilibrium diagram for Ni in Na_2SO_4 [8], it is believed that the pO^{2-} of Na_2SO_4 in air prior to reaction with pure Ni is about 9·5. NaCl addition to the sulphate will increase the pO^{2-} of the melt. Therefore, as can be seen from Fig. 3 of [8], the Ni_3S_2 region is thermodynamically favoured (for pO^{2-} values from about 10–12) and an equilibrium Ni/NiO/Ni_3S_2 is also possible (for a fixed value of E and pO^{2-}). Even if Ni_3S_2 is not found among the reaction products, liquid phases might be formed from the Ni_3S_2/Ni eutectic (m.p. 637° C), which can accelerate the destruction if the corrosion conditions are prolonged.

(c) At potentials resulting in full passivation of Ni smooth dissolution occurs both in the presence and absence of sodium chloride as a result of the formation of a protective oxide film on the whole surface.

(d) Evidence of extensive intergranular attack

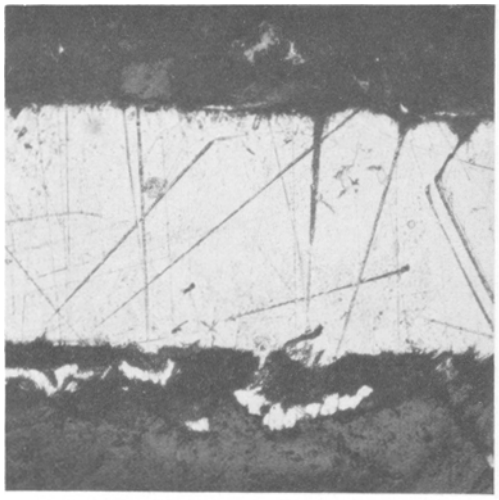

Fig. 30. Ni, Na_2SO_4, conditions as in Fig. 29, section (× 152): corroded surface showing islands of unreacted nickel.

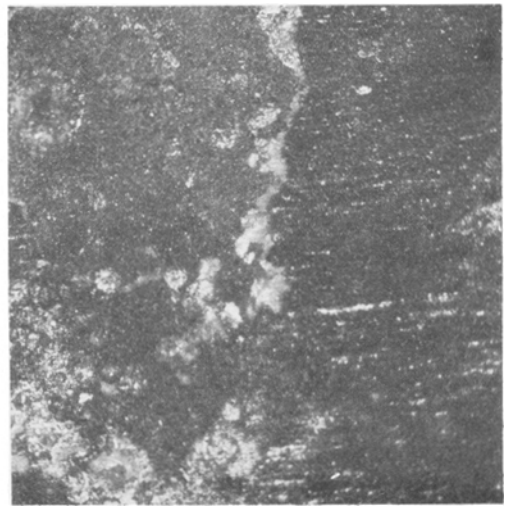

Fig. 32. Dissolution of Ni at a potential just above the passive potential range (— 0·5 V) in Na_2SO_4 at 900° C, in air (C, Fig. 28). Surface (× 35).

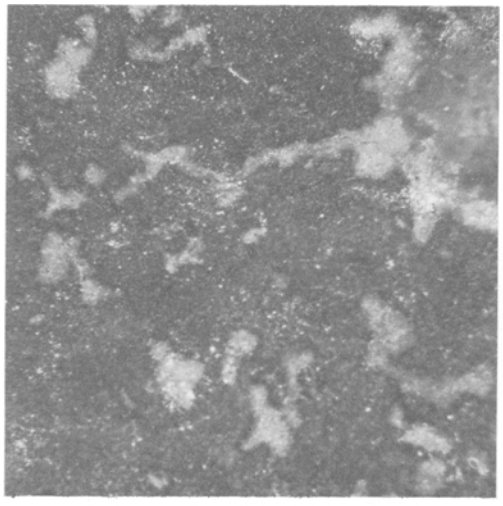

Fig. 33. Dissolution of Ni in the transpassive area (— 0·1 V) in Na_2SO_4 at 900° C, in air (D, Fig. 28). Surface (× 35).

Fig. 35. Dissolution of Ni in the transpassive are (— 0·2 V) in Na_2SO_4–15% NaCl at 900° C, in air (F, Fig. 28). Surface (× 35).

was detected on Ni after tests in pure NaCl. The intergranular attack is possible due to the chloride ions acting selectively on some crystallographic planes more than others. The nickel ion content of the melt is continuously reduced by $NiCl_2$ evaporation, corrosion being self-sustained. Indeed Ni and Cl were found at the top of the reaction cell in which Ni had been exposed to Cl-melts

(e) In general higher-content SO_3 atmospheres are more corrosive for Ni than is pure air. S penetration was detected which might be the reason for the Ni embrittlement. In addition the SO_3 pressures might stabilize the sulphate melt at a high pO^{2-} value and therefore enhance the Ni dissolution as can be seen from Fig. 3 of [8]. 0·05–0·5 wt% Ni was found in a residual melt of Na_2SO_4 under 5×10^{-5} atm SO_3 in contrast with a melt of Na_2SO_4 under air where no Ni was found.

Fig. 34. Dissolution of Ni in the active potential range (— 0·85 V) in Na_2SO_4–15% NaCl at 900° C, in air, (E, Fig. 28). Surface (× 35).

4. Summary and conclusions

(a) The electrokinetic behaviour of nickel electrodes in molten sodium sulphate at 900° C, in air, is characterized by three different regions. The first region corresponds to the onset of passivity and consists of the simultaneous nickel dissolution and passivation; the second is related to the dissolution of passive nickel; and the third corresponds to the local oxidation of passive nickel and sulphate discharge. The passive film on Ni is mainly NiO.

(b) The E–i curves for nickel in Na_2SO_4–NaCl melts, in air, in the range 0–80% NaCl, which are similar to the anodic polarization curve for Ni in pure Na_2SO_4, show that halide additions (especially those up to 25%) strongly affect the anodic behaviour of Ni in the active region and have practically no effect on the passive region. These higher dissolution rates are represented by the equation

$$Ni_3S_2 + 4NaCl + 1/2O_2 = 2NiCl_2 + 2Na_2S + NiO$$

which is also suggested to be a critical factor in the Ni passivation. Careful analysis of the transpassive part of the polarization curves also showed that the overpassive dissolution current is smaller in Cl^- melts than in SO_4^{2-} alone. This was further evidenced by particular experiments which have been concerned with determining the inhibiting role of NaCl on Ni in the passive–transpassive area.

(c) The passive capability found for Ni in Na_2SO_4/NaCl melts, in air, is destroyed by SO_3 atmospheres. The high rates of corrosion observed at high partial pressures of SO_3 are shown to be mainly due to the effect of SO_3 on the solubility of the corrosion products.

(d) The high dissolution rates and the shape of the polarization curves for Ni in pure NaCl at 900° C, in air, indicate that this material is typically active in the NaCl electrolyte. Metal dissolution must occur at the expense of a simultaneous reduction of Na^+ ions to Na_2^+ subions, accompanied by the corrosion of the metal interacting with the dissolved oxygen and the chloride ions, as well as with the chlorine and oxide ions formed in the reaction of oxygen with chloride ions.

(e) The potential decay curves for Ni in Na_2SO_4–NaCl melts show that thin passive films are very sensitive to Cl^- attack, but once a thick oxide film forms on the specimen, the Cl^- addition is accompanied by an increase in the film stability. Hence, there appears to be no simple correlation between the ease of achieving passivity (more likely in pure Na_2SO_4) and the stability of the passive film (enhanced in Cl^--melts).

(f) Topochemical studies of the corrosion products of the Ni, Na_2SO_4–NaCl reactions are in good agreement with the electrochemical results.

Acknowledgements

This work has been carried out with the support of Procurement Executive, Ministry of Defence, UK, and the authors acknowledge some useful discussions with Mr J. F. G. Condé and Mr G. C. Booth of that organization. One of us (C. A. C. S.) is also grateful to Instituto de Alta Cultura (Lisbon) for a bursary.

References

[1] C. A. C. Sequeira and M. G. Hocking, *J. Appl. Electrochem.* 8 (1978) 145.
[2] K. Arnold and K. J. Vetter, *Z. Elektrochem.* 64 (1960) 407.
[3] G. Okamoto and N. Sato, *J. Electrochem. Soc. Japan* 27 (1959) E-125.
[4] *Idem, J. Electrochem. Soc.* 110 (1963) 605.
[5] L. F. Trueb, G. Trumpler and N. Ibl, *Helv. Chim. Acta* 44 (1961) 960.
[6] W. J. Muller, 'Die Bedeckungstheorie der Passivitat der Metalle', Berlin (1933).
[7] H. Gerischer, *Agnew. Chem.* 70 (1958) 285.
[8] C. A. C. Sequeira and M. G. Hocking, *Brit. Corrosion J.* 12 (1977) 158.
[9] H. Lux, *Z. Elektrochem.* 45 (1939) 303.
[10] H. Flood, T. Forland and K. Motzfeldt, *Acta Chem. Scand.* 6 (1952) 257.